Journal of
Manufacturing and Materials Processing

MDPI

Article

Predicting the Ultimate Tensile Strength of Friction Stir Welds Using Gaussian Process Regression

Roman Hartl *, Fabian Vieltorf, Maximilian Benker and Michael F. Zaeh

Institute for Machine Tools and Industrial Management (*iwb*), Technical University of Munich, Boltzmannstr. 15, 85748 Garching, Germany; fabian.vieltorf@iwb.tum.de (F.V.); maximilian.benker@iwb.tum.de (M.B.); michael.zaeh@iwb.tum.de (M.F.Z.)

* Correspondence: roman.hartl@iwb.tum.de; Tel.: +49-(0)89-289-15483

Received: 29 June 2020; Accepted: 20 July 2020; Published: 22 July 2020

Abstract: In the work described here, Gaussian process regression was applied to predict the ultimate tensile strength of friction stir welds through data evaluation and to therefore avoid destructive testing. For data generation, a total of 54 welding experiments were conducted in the butt joint configuration using the aluminum alloy EN AW-6082-T6. Four tensile samples were taken from each of the 54 experiments and the resulting ultimate tensile strength of the weld seam segment was modeled as a function of the weld's surface topography. Further models were created for comparison, which received either the process variables or the process parameters to predict the ultimate tensile strength. It was shown that the ultimate tensile strength can be accurately predicted based on the weld's surface topography. Especially for low welding speeds, the correlation coefficients between the true and the predicted ultimate tensile strength were high. However, overall, even higher correlation coefficients could be achieved when providing the process variables or the process parameters to the model. In conclusion, it was shown that the developed Gaussian process regression model is a powerful approach for replacing destructive testing and for predicting ultimate tensile strength based solely on data that can be collected non-destructively.

Keywords: friction stir welding; machine learning; Gaussian process regression; non-destructive testing; surface inspection

1. Introduction

Friction stir welding (FSW) produces welds by using a rotating, non-consumable welding tool to locally soften a workpiece using heat that is generated through friction and plastic work [1]. Ever since Thomas [2] first demonstrated friction stir welding in 1991, its application has been steadily growing throughout the industry [3]. With the use of FSW soaring, there is an increasing need for non-destructive testing (NDT) processes that are superior to those currently available on the market in order to provide adequate quality inspection, particularly for safety-critical applications [3]. The destructive evaluation of friction stir welds is not recommended in most cases because it is expensive both in terms of lost workpieces and time-consuming execution [4]. The NDT requirements for assessing the weld quality expressed by the industry are short execution times and cost-efficiency [3]. The ability to reliably detect small defects and determine the associated mechanical properties for products that are joined using FSW is important for maintaining quality assurance and for complying with defined standards [3]. NDT methods can be classified as either direct or indirect methods [5]. The direct methods make use of techniques, such as camera vision or radiography. They are based on dimensional measurements and have a high degree of accuracy, however, due to numerous practical limitations, such as the positioning of the sensors in an environment with exposure to vibrations and improper illumination, the direct methods are often limited to laboratory use [5]. In order to overcome problems

typically associated with direct monitoring, indirect systems have been developed in the field of FSW that sense physical quantities, such as current, force, torque, acceleration and temperature. These systems are less accurate compared to the direct methods of monitoring but are economically and practically more suitable for industrial use [5].

In the field of friction stir welding, efforts have been made to predict the mechanical properties of the joint from non-destructively acquired information. Analytical models [6] and empirical models (e.g., artificial neural networks (ANNs) [7]), have been used to predict the mechanical properties. Verma et al. [8] investigated the potential of machine learning methodologies apart from ANNs for predicting the ultimate tensile strength of friction stir welds. Gaussian process regression (GPR) [9], support vector machines (SVM) [10], and the multi-linear regression (MLR) [11] were applied. Two different covariance functions were used for the GPR and the SVM—the radial basis function (RBF) [9] and the Pearson VII universal kernel (PUK) [12]. The two process parameters of welding speed and tool rotational speed were utilized as input data for the model. The output variable was always the ultimate tensile strength. For data generation, the two factors of welding speed and tool rotational speed were varied over five steps each in a full factorial experimental design. Out of the 25 welds, 83% (19 samples) were assigned to the training data set and the remaining 17% (6 samples) were assigned to the test data set. The Pearson correlation coefficient (PCC) and the root mean square error (RMSE) between the true and predicted ultimate tensile strength were employed as performance indicators. The GPR in combination with the RBF covariance function performed the best out of the five models tested. A PCC of 0.97 and an RMSE of 5.94 MPa were achieved for the six test samples. Verma et al. [8] have thus shown that using the GPR is well suited for non-destructively predicting ultimate tensile strength at FSW. However, Verma et al. [8] only used the two process parameters of welding speed and tool rotational speed as inputs for the machine learning models to predict ultimate tensile strength. Process information, which can be collected through direct or indirect NDT methods, was not provided for the model, but this allowed higher accuracies of the models to be achieved, and the trained models transferred more easily to other welding tasks without requiring new training.

According to Zuo et al. [13], the surface topography of friction stir welds plays an important role in the quality of the joints. It was proven that the two process parameters of welding speed and tool rotational speed have an influence on the semicircular surface texture that is typical for friction stir welds. To record the surface topography of welds inline or offline, there are numerous systems available based on the principle of laser triangulation [14]. Hartl et al. [15] defined key indicators for quantifying the surface topography at FSW and demonstrated that some of these indicators can be predicted by evaluating process variables that are recorded during welding [16]. Furthermore, it has already been demonstrated that, for low welding speeds, there are correlations between the surface topography and the ultimate tensile strength of friction stir welds for a wide range of tool rotational speeds. In investigations conducted by Hartl et al. [17], a correlation of −0.90 between the seam underfill of the welds and their ultimate tensile strength was obtained for a welding speed of 500 mm/min. The correlation between the flash height and the ultimate tensile strength was −0.84. However, data regarding the surface topography of friction stir welds seem to have not been used to estimate their ultimate tensile strength so far.

The purpose of this work was to study whether it is possible to estimate the ultimate tensile strength of friction stir welds by applying Gaussian process regression and provide surface topography data to the model. The GPR was selected primarily for the following three reasons:

- Due to the flexibility in modeling, since GPR is a non-parametric method [9].
- Due to the possibility of quantifying uncertainties for the prediction, which can be a great benefit for safety-critical applications [9].
- Since Verma et al. [8] compared the performance of the GPR to predict the ultimate tensile strength based on the process parameters with the multi-linear regression and support vector machines—the GPR led to the best results.

The results gained by using the surface topography data as input information had to be compared to the results in case process variables (e.g., process forces and temperatures) or process parameters (welding speed and tool rotational speed) are used as input data. It also had to be examined whether the use of more complex covariance functions, such as compositional structures introduced by Duvenaud et al. [18] (hereafter called additive GP or Add) or the spectral mixture (SM) covariance function introduced by Wilson et al. [19], leads to an improvement over simpler covariance functions, such as the RBF, the rational quadratic (RQ), or the Matérn 5/2 (Mat 5/2) covariance function. The fundamentals of the GPR are described in detail in Rasmussen et al. [9] and are briefly presented in Appendix B of the present work.

2. Materials and Methods

2.1. Welding Experiments

The experiments were performed on a four-axis milling center adapted for FSW. Each weld had a length of 205 mm and combined two sheets of the aluminum alloy EN AW-6082-T6 in the butt joint configuration. The chemical composition of the used material was specified by the selected supplier Bikar Metalle GmbH (Bad Berleburg, Germany), as listed in Table 1. The designation "*T6*" implies that the material was solution heat-treated and then artificially aged [20].

Table 1. Chemical composition of the used material EN AW-6082-T6 in %, which was reported by the selected material supplier, Bikar Metalle GmbH (Bad Berleburg, Germany).

Si	Fe	Cu	Mn	Mg	Cr	Zn	Ti	Others
0.90	0.42	0.10	0.44	0.70	0.03	0.13	0.03	max. 0.05

Each individual sheet had a dimension of 325 mm × 88.5 mm. The sheet thickness t was 4 mm, as shown in Figure 1.

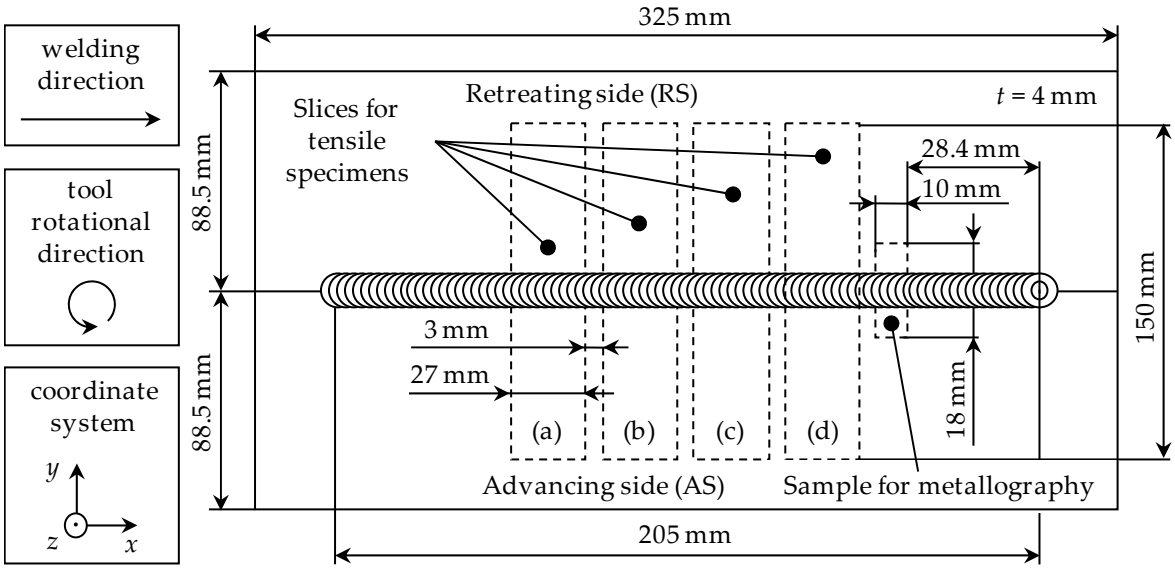

Figure 1. Sheet metal configuration in the butt joint with sampling areas for the material tests.

The process forces in three spatial directions F_x, F_y, and F_z, and the spindle torque M_z were recorded with a sampling rate of 9.6 kHz by a dynamometer, which is described in more detail in Krutzlinger et al. [21]. The temperatures at the tool shoulder T_S and the tool probe T_P were measured by thermocouples with a sampling rate of 220 Hz. The temperature measuring system was based on the one described by Costanzi et al. [22]. The accelerations a_x, a_y, and a_z in three spatial directions with

a sampling rate of 20 kHz were acquired by an acceleration sensor type 8762A50 of Kistler Instrumente GmbH (Winterthur, Switzerland). The accelerometer was positioned 20 mm away from the immersion point of the welding tool during the experiments. A two-piece tool with a concave shoulder with a radius r_S of 7 mm and a conical probe with a radius r_P of 3 mm was utilized. The probe had a M6 thread and three flats. The tool geometry and the most important dimensions are presented in Figure 2 and Table 2.

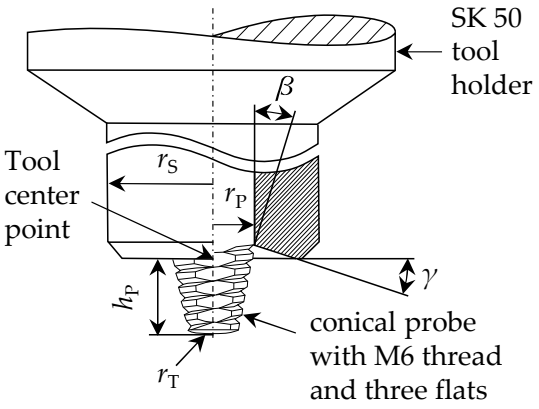

Figure 2. Tool geometry with the most important dimensions (adapted from Bachmann et al. [23]).

Table 2. Dimensions of the used tool.

Geometry Feature	Value
Probe radius r_P	3 mm
Shoulder radius r_S	7 mm
Conical probe angle β	10°
Probe length h_P	3.75 mm
Probe tip radius r_T	10 mm
Concave shoulder angle γ	10°

The experiments were performed in position-controlled operation with an immersion depth of 0.1 mm and a tool tilt angle of 2°. The dwell time at the immersion point was one second. The welding speed v_s and the tool rotational speed n (r/min rate) were modified. The examined welding speeds were 500 mm/min, 1000 mm/min and 1500 mm/min. As high welding speeds are becoming increasingly important for industrial applications, especially in the context of electromobility [24], welding speeds of up to 1500 mm/min were applied The ratio between the tool rotational speed and the welding speed n/v_s was varied over a wide interval from 1 mm^{-1} to 7 mm^{-1}. Furthermore, the tool rotational speed did not exceed 5000 min^{-1}. Exceeding these boundaries could have damaged the welding tool or the measuring equipment. To generate a sufficient amount of data, the tool rotational speed was adjusted in steps of 200 min^{-1} within the mentioned boundaries, which resulted in an experimental design totaling 54 experiments. Table A1 in Appendix A shows the process parameters applied in each welding process.

Figure 1 displays the areas of removal of the four slices (a)–(d) for the tensile specimens. Since four tensile specimens were taken from each of the 54 manufactured welds, a total of 216 tensile specimens were available. In order not to change the weld seam surface, the tensile specimens were prepared to the correct geometry for the tensile tests after scanning the surface topography of the 216 slices. The dimensions of the tensile specimens are illustrated in Figure 3a. The topography of the welds was examined using a three-dimensional profilometer VR-3100 (Keyence Deutschland GmbH, Neu-Isenburg, Germany). Thereby, white LEDs projected light from two places onto the weld and the reflected light was measured by a CMOS sensor. The smallest measurable difference in the z-direction, as shown in Figure 1, was 1 µm. The sheet surface was always defined as the zero height. The distance between

the individual topography points in the *x*-*y*-plane was approximately 24 µm. Consequently, a total of about 470,000 topography points were generated for the area (A), as shown in Figure 3a, containing the weld seam on the 15-mm-wide tensile specimens.

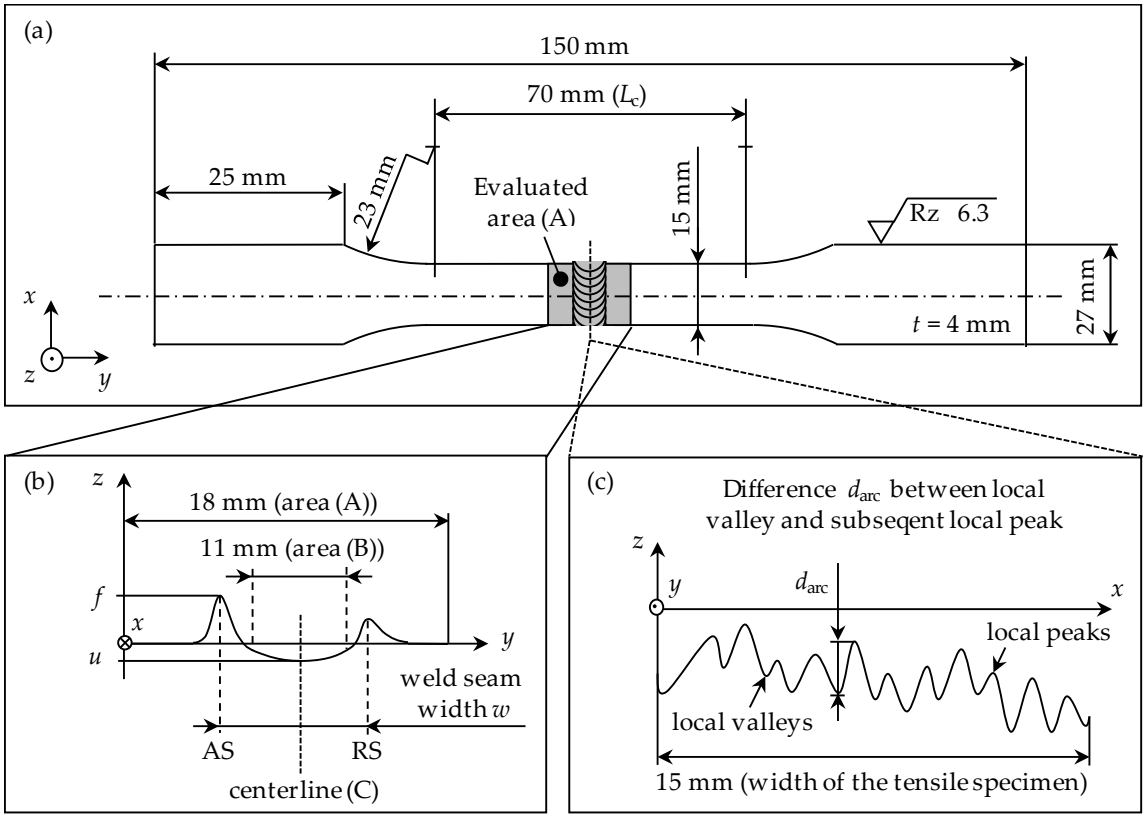

Figure 3. (**a**) Geometry and dimensions of the tensile specimens; (**b**) Evaluated surface topography; (**c**) Topography along the centerline of the weld.

The key indicators to quantify the flash formation and the weld seam width were calculated by using area (A), the key indicators for the seam underfill were specified by using area (B), and the arc texture formation was characterized along the weld centerline (C), as shown in Figure 3b,c. Figure 3b schematically shows the flash height f, the seam underfill u and the weld seam width w for a section of the weld surface. The weld seam width w was defined as the distance between the two peaks of the flash formation on the advancing side (AS) and on the retreating side (RS). Due to the distance of the topography points of approximately 24 µm, there were 625 sections of the weld's topography for each of the 15-mm-wide tensile specimens. From the corresponding 625 values for the flash height f, the seam underfill u, and the weld seam width w, the mean values for the flash height f_m and the seam underfill u_m, as well as the standard deviations of the flash height S_f, of the seam underfill S_u, and of the weld seam width S_w were calculated. Figure 3c schematically shows the topography along the weld centerline (C). Due to the seam underfill, the topography along the centerline is usually below the sheet surface. The number of local valleys and local peaks along the centerline was counted (n_{count}) and compared with the theoretical number ($n_{theoret}$), which leads to the ratio r_{arc}:

$$r_{arc} = \frac{n_{count}}{n_{theoret}} \quad (1)$$

The theoretical number n_{theoret} was calculated using the tool rotational speed n, the welding speed v_s, and the width of the tensile specimen, which was 15 mm:

$$n_{\text{theoret}} = \frac{n}{v_s} \cdot 15 \text{ mm} \quad (2)$$

In addition, for each tensile specimen the standard deviation S_d of the differences d_{arc} between the local valleys and the subsequent local peaks were calculated along the 15-mm-long centerline (C) of the tensile specimens. The peak material volume V_{mp} [25] was determined for area (B) of each tensile specimen. In a previous study it was found that, by employing the peak material volume V_{mp}, the surface galling of the weld can be quantified [15]. The eight topography indicators utilized to quantify the 15-mm-long weld surface segment on the tensile specimens are summarized in Table 3. These values were later used as input variables for the Gaussian process regression model to predict the ultimate tensile strength based on the weld topography.

Table 3. Key indicators for quantifying the surface topography of the 15-mm-long weld sections on the tensile specimens.

Surface Feature	Key Indicator 1	Key Indicator 2
Flash formation	Mean flash height f_m	Standard deviation of the flash height S_f
Seam underfill	Mean seam underfill u_m	Standard deviation of the seam underfill S_u
Weld seam width	Standard deviation of the weld seam width S_w	-
Arc texture formation	Ratio between the counted and the theoretical number of local valleys and peaks along the weld centerline r_{arc}	Standard deviation of the differences between the local valleys and the subsequent local peaks along the weld centerline S_d
Surface galling	Peak material volume V_{mp}	-

The signals of the nine different recorded process variables (F_x, F_y, F_z, M_z, T_P, T_S, a_x, a_y, a_z) were filtered, cut, and assigned to the corresponding weld segments of the tensile specimens. Afterwards, the following ten statistical values were calculated for each process variable corresponding to the 216 weld segments: arithmetic mean, maximum, minimum, median, root mean square (RMS), variance, kurtosis, skewness, highest amplitude in the frequency spectrum after performing a fast Fourier transform, and the span between the maximum and the minimum signal value of each segment. Thus, a total of 90 different features (nine process variables times ten statistical values) were available for each of the 216 tensile specimens. Some of these values were later provided as inputs for the Gaussian process regression model to predict the ultimate tensile strength based on the process variables.

A period of 7.5 weeks was scheduled between the welding process and the tensile tests. Based on the findings of Brenner et al. [26], it was assumed that the metallurgical transformations were completed after this period. For the tensile test, a Z050 AllroundLine material testing machine (ZwickRoell GmbH & Co. KG, Ulm, Germany) was utilized. In addition to the 216 tensile specimens for the welds, ten tensile tests were conducted on specimens with the base material for reference. The geometry of the tensile specimens corresponded to the specifications of DIN 50125, Form E [27]. All tensile tests were performed according to the standards DIN EN ISO 4136 [28] and DIN EN ISO 6892-1 [29]. According to the recommendation of the standard DIN EN ISO 6892-1 [29], the test speed was set to 0.0067 1/s to determine the ultimate tensile strength.

Metallographic specimens were prepared to inspect the welds for internal defects. After taking the samples for metallography from the welded parts, as shown in Figure 1, they were embedded in an epoxy resin, ground to a fineness of P1200, polished with a 3 µm diamond suspension, and then finely polished with colloidal silica. Finally, the samples were etched with Kroll's etchant, which is described in Vander Voort [30].

The values for the eight surface topography indicators, as shown in Table 3, as well as the ultimate tensile strengths of the 216 tensile specimens, are given in the Supplementary Materials to the article.

2.2. Application of the Gaussian Process Regression

For the present work, the Gaussian process regression model, as described in Appendix B, was applied. The experimental data were stored in a $D \times q$ design matrix X, where q represented the number of observations and D corresponded to the total number of features which are, for example, the mean flash height f_m, the mean z-force $F_{z,m}$ or the tool rotational speed n. The mean function $m(\mathbf{x})$ was set to zero, which is a common choice when modeling with Gaussian processes [9]. As a consequence, the data were normalized to mean zero and to variance one before performing the regression. The data were divided into 80% training data and 20% test data. The distribution of the data between the two data sets was random. Following Rasmussen et al. [9], a five-fold cross-validation was applied.

Five different covariance functions were tested: RBF, RQ, Matérn 5/2, additive GPs, and SM. The covariance functions are described in Appendix B. For the RBF, the RQ, and the Matérn 5/2 covariance function, the automatic relevance determination (ARD) variant was used (see Equation (A19) in Appendix B). For the application of the additive GP according to Duvenaud et al. [18], it was necessary to define the base covariance function and the maximum order up to which calculations should be performed. The RBF covariance function was employed, and the maximum order was set to the maximum number of dimensions D. For the use of the SM covariance function as described by Wilson et al. [19], the choice of an integer parameter Q for the maximum number of mixture components was necessary. All possible models for a Q from 1 to 20 were calculated and the model with the lowest mean absolute error (MAE) was chosen. In order to learn sensible model parameters, gradient-based optimization of the logarithmic marginal likelihood was performed. To avoid getting stuck in local optima, the process of model fitting was repeated ten times. In each iteration, the initial values of the hyperparameters were randomly set between e^0 and e^{10}, and afterwards, the model with the lowest MAE for predicting the ultimate tensile strength of the specimens contained in the test data set was applied.

The performance measure ultimately utilized to evaluate the deviation between the predicted and the true ultimate tensile strength was the Pearson correlation coefficient (PCC) [31]. Using the PCC proved to be the best way to compare the results obtained with the different input data for the model and the different covariance functions that were employed. As a benchmark for the GPR, a multi-linear regression (MLR) [31] was conducted using the same input data, respectively. In the MLR, a division of the data set into 80% training data and 20% test data was implemented as for the GPR by using a fivefold cross-validation.

The computations were performed on the CPU, which was an Intel® Core™ i7-6700HQ CPU at 2.60 GHz. The installed RAM was 16 GB.

3. Results

Training the algorithm and predicting the ultimate tensile strength were performed separately for the three different welding speeds of 500, 1000, and 1500 mm/min, as well as for the combined data using all three welding speeds. In the following paragraphs, not all achieved results with all five employed covariance functions are given. Instead, only the best result and the corresponding covariance function are presented. The mean of the ten reference tensile specimens for their measured ultimate tensile strength was 332.97 MPa at a standard deviation of 1.15 MPa.

3.1. Prediction of the Ultimate Tensile Strength Using Surface Topography Data

All eight surface topography indicators (f_m, S_f, u_m, S_u, S_w, r_{arc}, S_d, V_{mp}), described in Section 2.1, were used as input variables for the GPR model. The input matrix X thus had eight dimensions d in total. In the first step, the data from all 216 conducted tensile tests were utilized. Some outliers with significantly lower ultimate tensile strengths or very strong flash formation, which occurred especially at very high or very low tool rotational speeds n, were also included in the data. The results are displayed in Table 4. Overall, in the five-fold cross-validation, a mean PCC between the true

and the predicted ultimate tensile strength of 0.76 was achieved when the data from all three welding speeds were taken into account. The standard deviation of the five values was 0.17. This result was achieved when using the SM covariance function. The total computation time was 6953 s. This was the time for the training and the testing of the five-fold cross-validation. As described in the previous chapter, for each part of the cross-validation in another nested inner loop, a ten-fold calculation with different initial hyperparameters was performed. The highest mean PCC of 0.87 was achieved at a welding speed of 500 mm/min.

Table 4. Results for predicting the ultimate tensile strength R_m when using the surface topography indicators as inputs for the GPR model.

Welding Speed v_s	500 mm/min	1000 mm/min	1500 mm/min	All Data
PCC mean	0.87	0.79	0.80	0.76
PCC standard deviation	0.15	0.23	0.05	0.17
Best covariance function	Add	SM	Mat 5/2	SM
Computation time in s	152	1130	1017	6953

However, no pattern could be identified as to why different covariance functions led to the highest mean PCC at the different welding speeds. The differences for the achieved PCCs for the different covariance functions were mostly small. For example, in Figure 4, the comparisons for the PCCs means and standard deviations between the true and predicted ultimate tensile strength when using the data collected at all three welding speeds are displayed. As already presented in Table 4, the best result was achieved when using the SM covariance function. However, in Figure 4, it becomes evident that the PCCs were only slightly lower when using other covariance functions, but the computation time decreased considerably. Further investigations also showed that the calculation with the SM covariance function required the longest computing time. The results when using the MLR were significantly worse than when using the GPR throughout the entire work, which confirmed the results of Verma et al. [8].

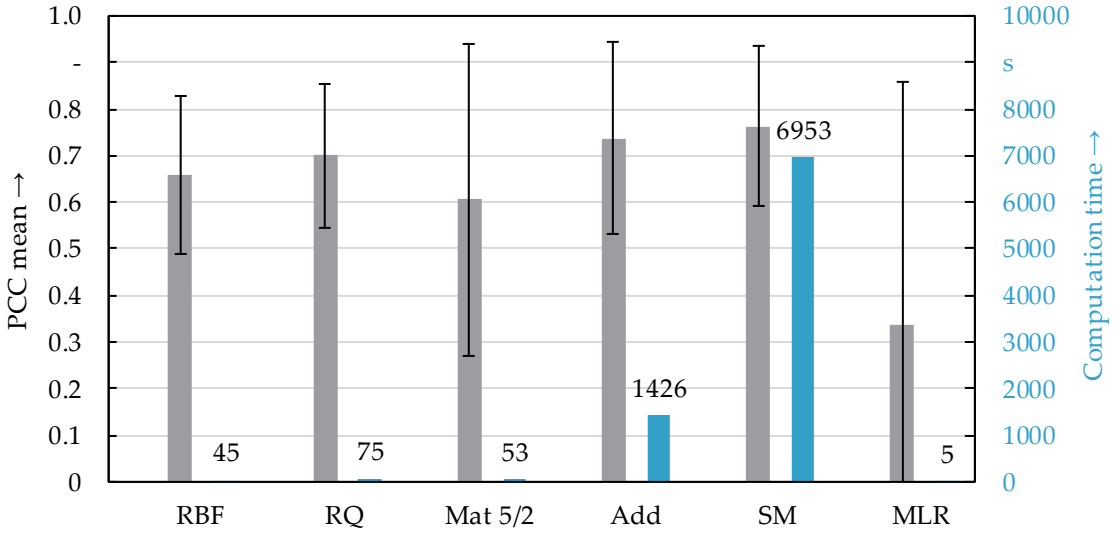

Figure 4. Comparison of the PCCs means and standard deviations for the different covariance functions and the MLR when using the topography information as input variables and providing the data collected at all three welding speeds. Additionally, the corresponding computation times are given.

Figure 5 illustrates the result when providing data from all three welding speeds and applying the SM covariance function. The results with (a) the lowest and (b) the highest correlation from the five-fold cross-validation are displayed. PCCs of 0.53 and 0.97 were achieved. In Figure 5b, it is demonstrated that the three outliers with an ultimate tensile strength of less than 175 MPa were

also very well predicted. In the result with the lowest PCC of 0.53, the two outliers with an ultimate tensile strength below 175 MPa were not well predicted. At extremely low or high tool rotational speeds, internal weld defects, such as tunnel errors, occurred. These considerably reduce the ultimate tensile strength and cannot be detected via the weld seam topography. This makes it difficult to predict the ultimate tensile strength and sometimes leads to low PCCs, as shown in Figure 5a.

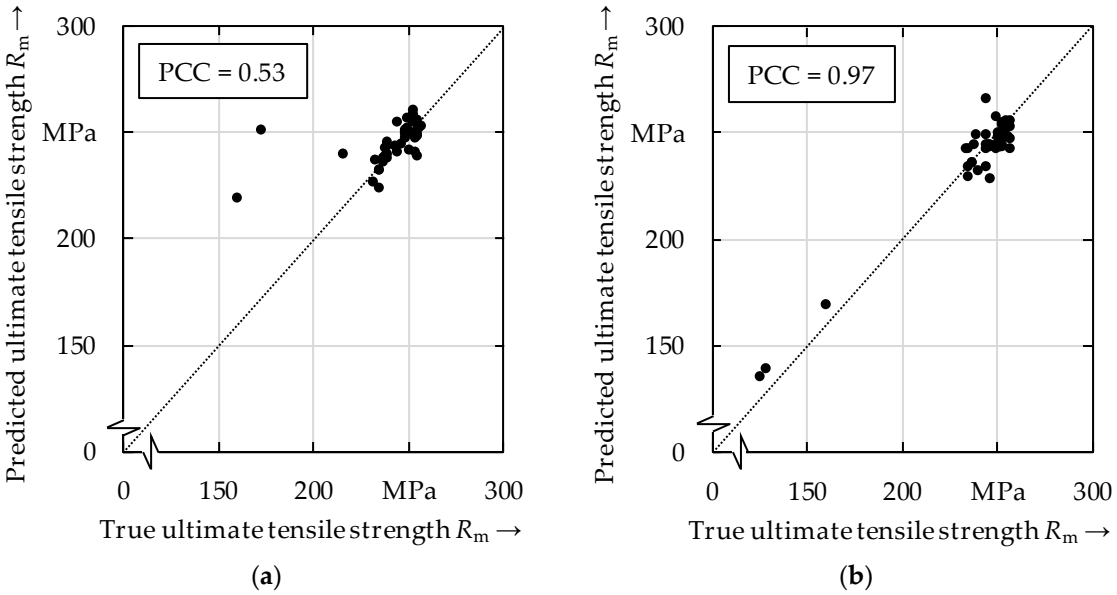

Figure 5. (**a**) The lowest and (**b**) the highest correlation out of the five-fold cross-validation to predict the ultimate tensile strength R_m, taking into account the surface topography data from all three welding speeds v_s and using the SM covariance function.

In the next step, some outliers were removed from the data set. These were the welds from experiments no. 1, 2, 3, 4, 5, 35, 36, 53 and 54, which were all experiments with extremely low or high tool rotational speeds, as shown in Table A1 in Appendix A. Extreme tool rotational speeds, as used in these experiments, lead to tunnel errors and other irregularities in the welds and are usually not employed in industrial applications. Table 5 shows that the PCCs significantly improved as a consequence. Using the data collected at all three welding speeds, the SM covariance function yielded a mean PCC of 0.96. The results presented in Tables 4 and 5 also demonstrate that the mean values for the PCC, when considering the individual welding speeds, tended to decrease as the welding speed increased. This is probably due to the fact that process stability and regularity decrease at higher welding speeds, making it more difficult to predict the ultimate tensile strength. The differences in the results between the various covariance functions were again small, as before, in the investigation with providing the outliers at extreme tool rotational speeds to the model. It was noticeable, however, that the SM covariance function again led to the best result when using all the data.

Table 5. Results for the prediction of the ultimate tensile strength R_m when using the surface topography indicators as input for the GPR model with outliers removed.

Welding Speed v_s	500 mm/min	1000 mm/min	1500 mm/min	All Data
PCC mean	0.94	0.93	0.83	0.96
PCC standard deviation	0.05	0.03	0.11	0.01
Best covariance function	Mat 5/2	Add	Add	SM
Computation time in s	28	203	179	4879

Figure 6 shows the worst and best results from the five-fold cross-validation when using the data from all three performed welding speeds. The five results ranged from a PCC of 0.95 to a PCC of 0.98,

which was assessed as a very high degree of reproducibility. The PCC standard deviation of the five calculations was 0.01, as shown in Table 5.

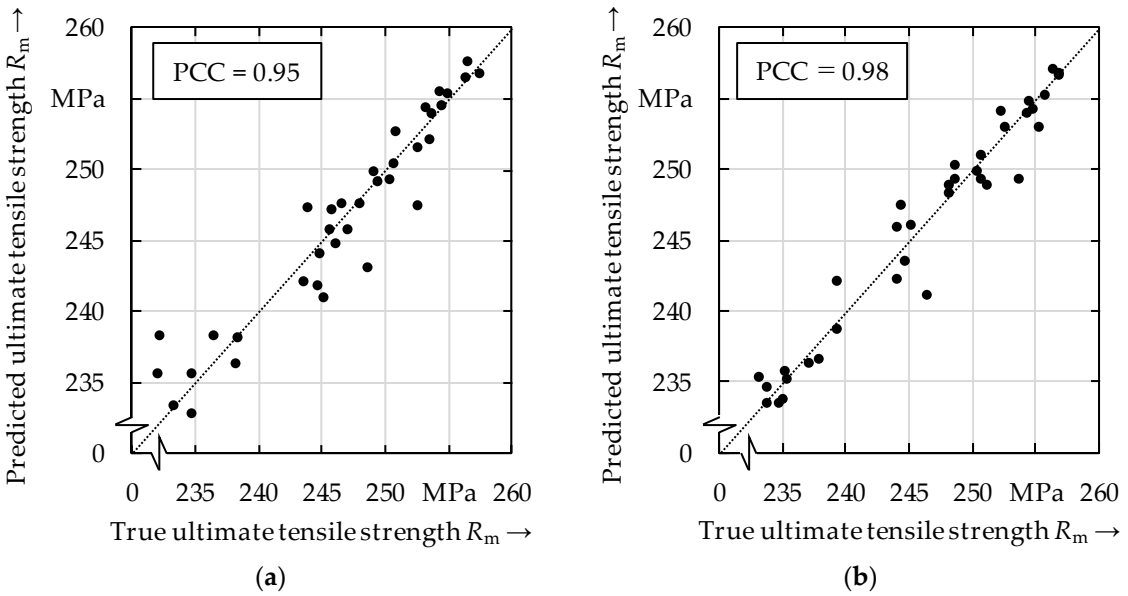

Figure 6. (**a**) The lowest and (**b**) the highest correlation out of the five-fold cross-validation to predict the ultimate tensile strength R_m taking into account the surface topography data from all three welding speeds v_s and using the SM covariance function. Additionally, some outliers were removed before training the GPR model in this case.

One advantage of using GPR is that it can specify a confidence interval for the prediction. This can be observed in Figure 7. For better visualization, only the data from the calculation with a welding speed v_s of 500 mm/min and the Matérn 5/2 covariance function were used to generate Figure 7. A mean PCC of 0.94 and a standard deviation of 0.05 were achieved in this way (see Table 5). In addition to the mean values of the predictions, the 95% confidence intervals are also given for the test samples.

Figure 7a,b show, again, the results with the lowest and highest PCC. It becomes clear that almost all true values are within the 95% confidence interval of the prediction. Especially for safety-critical applications, such as in the aerospace industry or electromobility, it might be interesting to provide a confidence interval for each weld segment within which the ultimate tensile strength is located with a certain probability.

Overall, it was proven that predicting the ultimate tensile strength in friction stir welding is possible when exclusively using surface topography information. However, there are also limits: the higher the welding speed is, the more erroneous the prediction. The reason for this is probably that the irregularity of the FSW process increases as the welding speed rises. Additionally, individual outliers in the measured data, for example, due to tunnel errors or sporadic irregularities in the recording of the surface topography, have reduced the achieved PCCs. By removing these outliers, which have always occurred at extreme tool rotational speeds that are of minor importance for industrial applications, the results could be improved significantly. The differences among the correlation coefficients between the true and the predicted values for the various covariance functions were low. It was noticeable, though, that when using the data for all three welding speeds, the SM covariance function always achieved the best results. However, the calculation time was also significantly higher than for the other covariance functions. This must be taken into account in a future application of the Gaussian process regression as an online monitoring system.

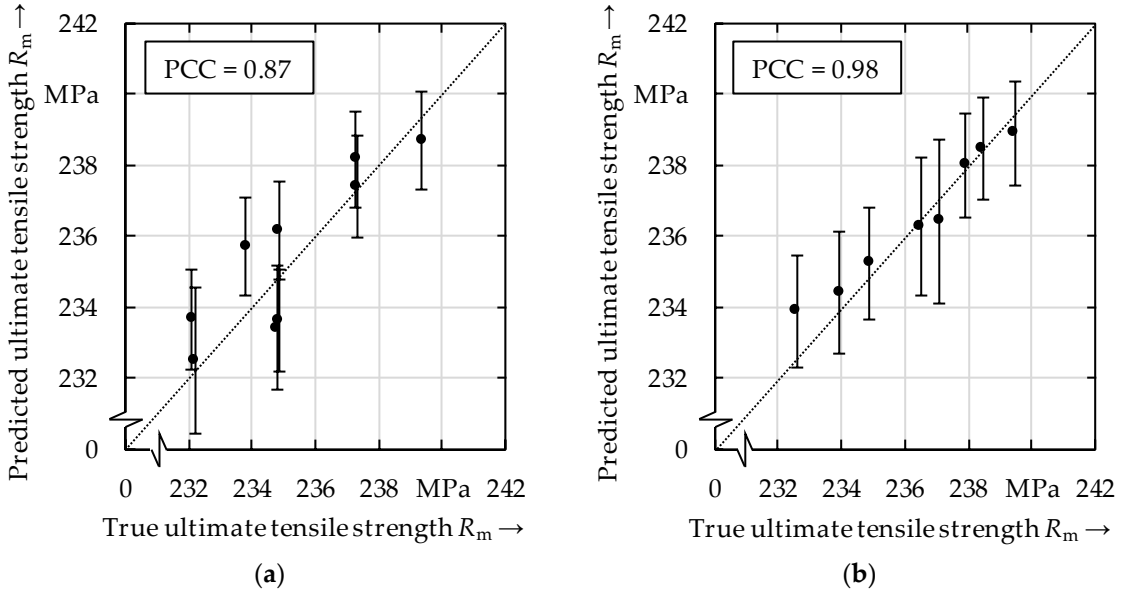

Figure 7. (**a**) The lowest and (**b**) the highest correlation out of the five-fold cross-validation to predict the ultimate tensile strength R_m at a welding speed v_s of 500 mm/min when using the surface topography data and the Matérn 5/2 covariance function. The graphs show the mean values of the predictions and the 95 % confidence intervals. In these investigations, some outliers were removed before training the GPR model.

3.2. Predicting Ultimate Tensile Strength Using Process Variables

For reasons of comparability, process variables were used as input data for the GPR model in the next step. As already described in Section 2.1, a total of nine different process variables (e.g., forces or temperatures), were recorded during the welding experiments. From each of these process variables, ten different statistical parameters were calculated. Thus, a total of 90 different features for the process variables were available for each of the 216 tensile specimens. In order to reduce the computing time, only the following six input dimensions were provided as input data for the model: the mean spindle torque M_z, the mean F_y-force, the mean F_z-force and the root mean square (RMS) values of the accelerations in x-, y-, and z-direction. These six input dimensions were determined based on a simple statistical analysis to assess which of the 90 different features have the highest correlation with the ultimate tensile strength.

The results in Table 6 were generated using all 216 tensile specimens from the 54 welding experiments. Outliers in the measurement data were not removed. The results listed in Table 6 demonstrate that the mean correlation coefficient PCC between the true and the predicted ultimate tensile strength was always above 0.90. Taking into account the data of all welding speeds, the mean PCC was 0.99 with a standard deviation of 0.01. Again, the best result for all welding speeds was generated using the SM covariance function. The significantly higher computation time of 6374 s, compared to the other results, which are listed in Table 6, resulted from the bigger data set and the use of the more complex SM covariance function. The quality of the prediction when using process variables thus exceeded the result when using the topography data as input variable. Furthermore, the model is less sensitive to outliers and therefore more robust when process-related features are integrated into the model.

Table 6. Results for the prediction of the ultimate tensile strength R_m when using process variables as input for the GPR model.

Welding Speed v_s	500 mm/min	1000 mm/min	1500 mm/min	All Data
PCC mean	0.99	0.91	0.93	0.99
PCC standard deviation	0.02	0.08	0.06	0.01
Best covariance function	Mat 5/2	RQ	Mat 5/2	SM
Computation time in s	27	32	30	6374

Figure 8 visualizes the predictions for the ultimate tensile strength for (a) the lowest and (b) the highest correlation between the true and predicted values from the five-fold cross-validation. It is evident that, in both diagrams, almost all points lie on the diagonal, indicating very good results in terms of high correlation coefficients PCC.

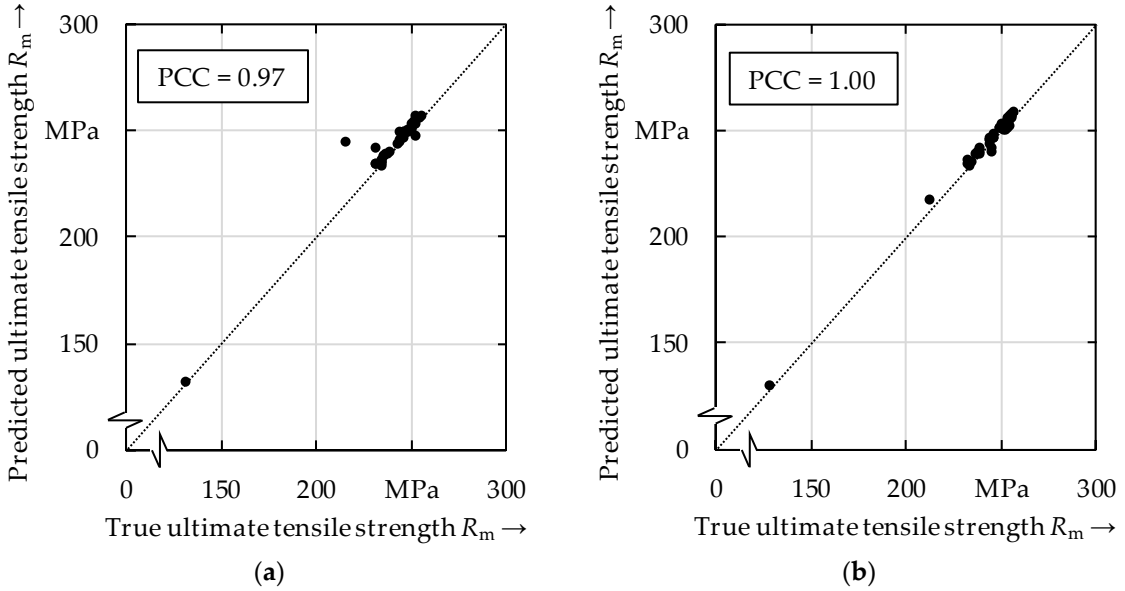

Figure 8. (**a**) The lowest and (**b**) the highest correlation out of the five-fold cross-validation to predict the ultimate tensile strength R_m, taking into account the process variable data from all three welding speeds v_s and using the SM covariance function.

Overall, the result for predicting the ultimate tensile strengths when evaluating the process variables exceeded the performance when using the topography data as the input variables. One explanation for this could be that the process variables can better represent the occurrence of internal defects, such as tunnel errors, than the surface topography data. Monitoring the surface topography can therefore not completely replace monitoring the process variables. Nevertheless, monitoring the surface topography can be a useful addition to an online monitoring system.

3.3. Predicting the Ultimate Tensile Strength Using Process Parameters

Finally, it was investigated which correlation coefficients PCC are achieved when using the two varied process parameters of welding speed and tool rotational speed as input information. When using all three welding speeds, both the welding speed and the tool rotational speed were utilized as input information. If the three welding speeds were considered individually, only the tool rotational speed was used as input information, so that only one input dimension d was provided. Again, all existing data were employed and outliers with a significantly lower ultimate tensile strength were not removed. Verma et al. [8] also used the two process variables of welding speed and tool rotational speed as input variables (see Section 1), whereby the six test samples yielded a correlation coefficient of

0.97 between the true and the predicted ultimate tensile strength when using the GPR with an RBF covariance function.

The results of the present work are listed in Table 7. The mean PCC from the five-fold cross-validation between the true and the predicted ultimate tensile strength was 0.99. This corresponds to the same result as when providing the process variables as input information. Additionally, the standard deviation was, once again, 0.01. When only using the data generated at a welding speed of 500 mm/min, a mean correlation coefficient PCC of 1.00 was achieved with a standard deviation of zero. When providing the process parameters as input data, it was also noticeable that two of the rather simpler covariance functions, RBF and RQ, led to the best results.

Table 7. Results for the prediction of the ultimate tensile strength R_m when using process parameters as inputs for the GPR model.

Welding Speed v_s	500 mm/min	1000 mm/min	1500 mm/min	All Data
PCC mean	1.00	0.88	0.94	0.99
PCC standard deviation	0.00	0.12	0.05	0.01
Best covariance function	RBF	SM	RQ	SM
Computation time in s	625	807	23	5761

Figure 9 visualizes the results for (a) the lowest and (b) the highest achieved correlation between the true and the predicted ultimate tensile strength from the five-fold cross-validation when using the SM covariance function. Most of the points are very close to the diagonal, which indicates good predictions.

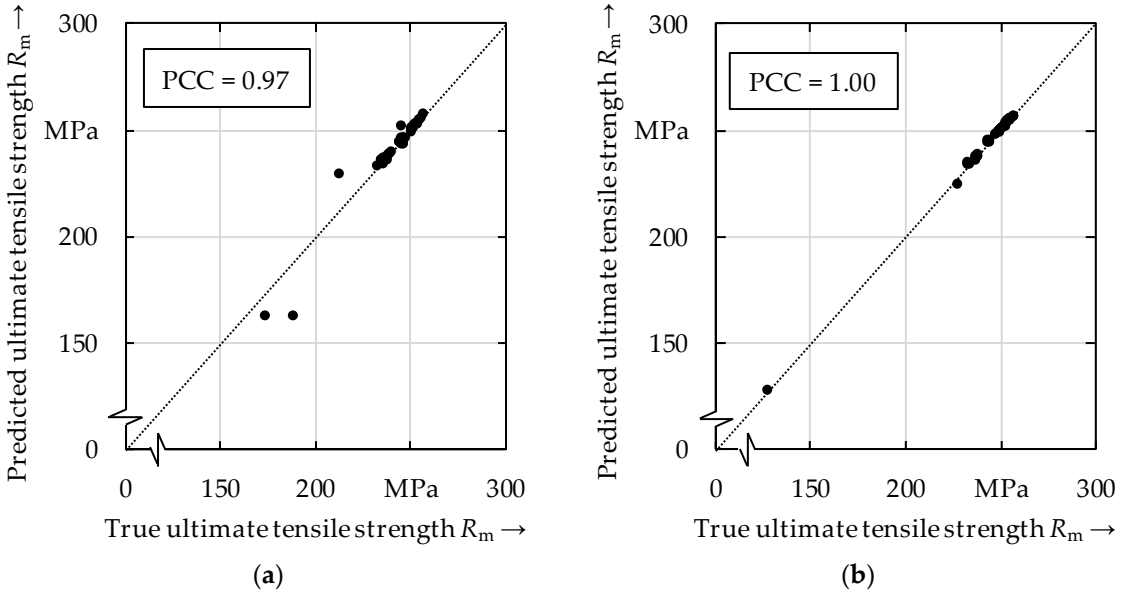

Figure 9. (**a**) The lowest and (**b**) the highest correlation out of the five-fold cross-validation to predict the ultimate tensile strength R_m, taking into account the process parameter data from all three welding speeds v_s and using the SM covariance function.

Since the tool rotational speed was the only input dimension when considering the individual welding speeds, the GP can be visualized for these cases. Figure 10 illustrates the mean value function and the 95% confidence interval for the ultimate tensile strength in dependence on the tool rotational speed. Figure 10a shows the graph when using the RBF covariance function and Figure 10b shows the graph for the SM covariance function. A difference between the two diagrams becomes clear when looking closely at the range between 1000 min^{-1} and 3500 min^{-1}. In Figure 10a, the width of the confidence interval is nearly constant, whereas in Figure 10b, the width

of the confidence interval varies in this range. In the ranges of the tool rotational speed that the model has not yet experienced, the width of the confidence interval increases. It seems plausible that predicting the ultimate tensile strength for unknown tool rotational speeds has a higher uncertainty than for tool rotational speeds that have already been tested. The SM covariance function is more flexible than the RBF covariance function and can probably, therefore, learn this uncertainty profile. Additionally, Figure 10 shows that the GPR models are able to reproduce the lower ultimate tensile strength at tool rotational speeds below 1000 min^{-1}, which was attributed to internal defects, such as tunnel errors.

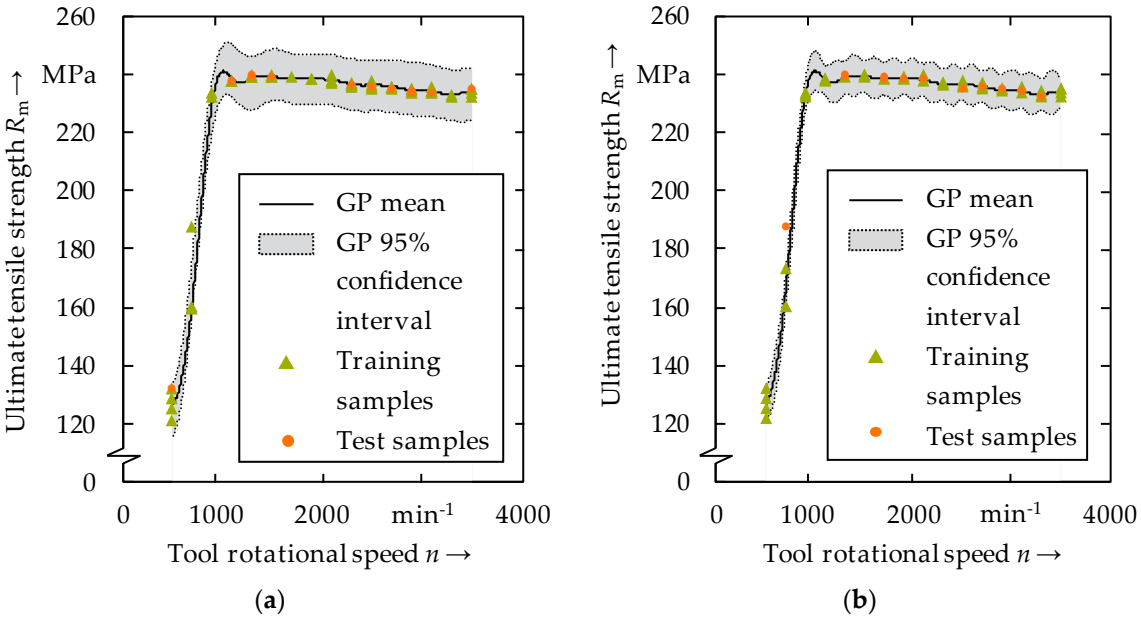

Figure 10. Visualization of the GP at a welding speed v_s of 500 mm/min with the tool rotational speed n as the only input dimension for the two covariance functions, (**a**) RBF and (**b**) SM.

Overall, predicting the ultimate tensile strength when utilizing the process parameters led to comparable PCCs, as when using the process variables.

4. Discussion

The conducted investigations demonstrate that it can be beneficial to evaluate the topography data of friction stir welds and this provides an additional possibility for online monitoring during friction stir welding for predicting the weld's ultimate tensile strength and the acceptability of the welded parts. Especially when no extreme tool rotational speeds are applied, the prediction of the ultimate tensile strength based on the surface topography shows good results. For safety-critical applications, such as in the aerospace industry or in electromobility, it might be interesting to monitor the weld's topography and supplement other usually applied monitoring systems, such as a force or torque monitoring system. However, when utilizing the process variables or the process parameters, the results for predicting the ultimate tensile strength were better than for the surface topography data. Additionally, the presence of typical defects of friction stir welds, such as tunnel errors, kissing bonds, or the lack of penetration defect probably cannot be detected by a topography monitoring system. Therefore, other monitoring systems cannot be completely replaced.

Whether there are pronounced correlations between the surface topography and weld defects, such as tunnel errors or kissing bonds, or between the surface topography and the microstructure of the weld, should be investigated more closely in future research work. Since the formation of the surface topography is presumably related to the welding temperature, which in turn is also connected to the weld's microstructure [32], correlations are conceivable, in particular, between

the surface topography and the microstructure. If significant correlations exist here, these could also be exploited to improve the monitoring of the FSW process.

A disadvantage of using the process parameters is assumed to be the lower degree of transferability of the trained model when applied to other welding tasks. However, further investigations are necessary to confirm the better transferability of the trained GPR model to other welding tasks when using the surface topography or process variables as input data. A disadvantage of using process variables compared to topography data is that they must be recorded during the process and cannot be determined subsequently. The weld's topography data can be determined offline at any time after the welding process. However, an advantage of the process variables compared to the topography data is that the required sensors (e.g., for recording forces or the spindle torque), are often already integrated in FSW systems. To record the surface topography of the welds, an additional sensor is necessary [14].

It was also remarkable that, when considering the data from all welding speeds, the SM covariance function always achieved the best result, as shown in Tables 4–7. It is therefore suspected that the more complex covariance functions (Add and SM) perform better than the simpler covariance functions (RBF, RQ, and Matérn 5/2) if there are more training data available and there are more input dimensions provided. However, this assumption also needs to be confirmed by further investigations. Since the computing time was by far the highest when using the SM covariance function, its online monitoring capability, which requires low computing times, must be evaluated in future research.

5. Conclusions

In the present work, a novel approach is proposed that estimates the ultimate tensile strength through a cost-efficient NDT method that is based on evaluating weld surface topography. For this purpose, a total of 54 welding experiments, which were performed at three different welding speeds, were evaluated. Four tensile samples were taken from each weld. By using Gaussian process regression and testing five different covariance functions, the ultimate tensile strength of friction stir welds was non-destructively assessed. Surface topography indicators were used as input data and the results were compared to cases in which process variables or process parameters were utilized as input data for the model. The achieved correlation coefficients PCC between the true and the predicted ultimate tensile strength when using the data from all welding speeds are summarized in Table 8.

Table 8. Summary of the achieved correlation coefficients between the true and the predicted ultimate tensile strength.

Input Variable	Surface Topography	Process Variables	Process Parameters
PCC mean	0.76	0.99	0.99
PCC standard deviation	0.17	0.01	0.01

By removing some outliers at very low or very high tool rotational speeds, the mean correlation coefficient PCC when providing the surface topography data to the model was improved to 0.96 with a standard deviation of 0.01.

The most important conclusions were:

- The Gaussian process regression is a powerful approach to non-destructively predict ultimate tensile strength through data evaluation. The uncertainty of the prediction can be quantified, and a confidence interval can be specified within which the ultimate tensile strength is located with a certain probability.
- It is possible to predict the ultimate tensile strength of friction stir welds by evaluating the surface topography through Gaussian process regression. This is especially valid for low welding speeds and when extremely low or high tool rotational speeds are not employed.

- The correlation coefficients for the prediction of the ultimate tensile strength by using the process variables or the process parameters were even higher compared to when using the surface topography data as inputs to the model.
- The differences in the PCCs for the various covariance functions used were low. However, when using the data from all investigated welding speeds, the spectral mixture covariance function according to Wilson et al. [19], always yielded the best results.

Supplementary Materials: The following are available online at http://www.mdpi.com/2504-4494/4/3/75/s1, Table S1: Values for the eight surface topography indicators listed in Table 3 and the ultimate tensile strengths for all 216 tensile specimens; the location of the individual slices a, b, c and d taken from the weld is specified in Figure 1.

Author Contributions: Conceptualization, R.H.; methodology, R.H.; software, R.H. and F.V.; validation, R.H., F.V. and M.B.; formal analysis, R.H. and F.V.; investigation, R.H. and F.V.; resources, R.H. and M.F.Z.; data curation, R.H. and F.V.; writing—original draft preparation, R.H. and M.B.; writing—review and editing, R.H.; visualization, R.H.; supervision, M.F.Z.; project administration, R.H. and M.F.Z.; funding acquisition, R.H. and M.F.Z. All authors have read and agreed to the published version of the manuscript.

Funding: The IGF research project no. 21,161 N of the "Research Association on Welding and Allied Processes of the DVS" has been funded by the AiF within the framework for the promotion of industrial community research (IGF) of the Federal Ministry for Economic Affairs and Energy on the basis of a decision by the German Bundestag.

Conflicts of Interest: The authors declare that they have no conflict of interest.

Appendix A Experimental Plan

Table A1. Welding experiments performed and mean ultimate tensile strength $\overline{R_m}$ achieved.

v_s = 500 mm/min				v_s = 1000 mm/min				v_s = 1500 mm/min			
Exp. no.	n min^{-1}	n/v_s mm^{-1}	$\overline{R_m}$ MPa	Exp. no.	n min^{-1}	n/v_s mm^{-1}	$\overline{R_m}$ MPa	Exp. no.	n min^{-1}	n/v_s mm^{-1}	$\overline{R_m}$ MPa
1	500	1.0	127	17	1100	1.1	245	37	1500	1.0	252
2	700	1.4	170	18	1300	1.3	247	38	1700	1.1	255
3	900	1.8	233	19	1500	1.5	248	39	1900	1.3	255
4	1100	2.2	238	20	1700	1.7	249	40	2100	1.4	254
5	1300	2.6	239	21	1900	1.9	250	41	2300	1.5	255
6	1500	3.0	239	22	2100	2.1	250	42	2500	1.7	256
7	1700	3.4	239	23	2300	2.3	251	43	2700	1.8	257
8	1900	3.8	238	24	2500	2.5	250	44	2900	1.9	257
9	2100	4.2	238	25	2700	2.7	249	45	3100	2.1	257
10	2300	4.6	236	26	2900	2.9	251	46	3300	2.2	255
11	2500	5.0	236	27	3100	3.1	249	47	3500	2.3	253
12	2700	5.4	236	28	3300	3.3	246	48	3700	2.5	254
13	2900	5.8	234	29	3500	3.5	246	49	3900	2.6	253
14	3100	6.2	234	30	3700	3.7	245	50	4100	2.7	250
15	3300	6.6	233	31	3900	3.9	244	51	4300	2.9	251
16	3500	7.0	234	32	4100	4.1	244	52	4500	3.0	253
	Average:		225	33	4300	4.3	247	53	4700	3.1	253
				34	4500	4.5	245	54	4900	3.3	248
				35	4700	4.7	236		Average:		254
				36	4900	4.9	225				
					Average:		246				

Appendix B Fundamentals of the Gaussian Process Regression

A Gaussian process (GP) is a distribution over functions. Formally, it is a collection of random variables that follow a joint Gaussian distribution and which are completely specified by the GP's mean function and covariance function [9]:

$$f(x) \sim \mathrm{GP}(m(\mathbf{x}), k(\mathbf{x}, \mathbf{x'})) \tag{A1}$$

whereby the mean function $m(\mathbf{x})$ and the covariance function $k(\mathbf{x}, \mathbf{x'})$ of a real process $f(\mathbf{x})$ are defined by [9]:

$$m(\mathbf{x}) \;=\; \mathbb{E}[f(\mathbf{x})] \tag{A2}$$

and

$$k(\mathbf{x}, \mathbf{x'}) \;=\; \mathbb{E}(f(\mathbf{x}) \;-\; m(\mathbf{x}))\cdot(f(\mathbf{x'}) \;-\; m(\mathbf{x'})) \tag{A3}$$

Consequently, any input $\mathbf{x}$ has a mean, which can be evaluated by the mean function. Furthermore, every two inputs $\mathbf{x}$ and $\mathbf{x'}$ have a common covariance that can be evaluated by the covariance function. If $\mathbf{x'}$ is equal to $\mathbf{x}$, the covariance function returns the variance of $\mathbf{x}$.

Assume a data set $\mathcal{D}$ with q observations:

$$\mathcal{D} \;=\; \left\{(\mathbf{x}_1\; y_1 \,\middle|\, i = 1, \ldots q)\right\} \tag{A4}$$

is given, where $\mathbf{x}$ is a D-dimensional input vector and y is a scalar output variable. All available data are aggregated in the $D \times q$ matrix X. The GP regression model with noise is given by:

$$\mathbf{y} = f(X) + \boldsymbol{\varepsilon} \tag{A5}$$

where $f(X)$ is a GP over the inputs X. The observed values y differ from the function values $f(X)$ by additive noise $\boldsymbol{\varepsilon}$ that follows an independent, identically distributed Gaussian distribution with zero mean and variance σ_ε^2 [9].

The data set $\mathcal{D}$ is divided into a training data set and a test data set. The training data are used for learning the GP model parameters. The already known training data are denoted by y at the inputs X and the unknown test data are denoted by $\mathbf{f}_*$ at the points X_*. When modelling with GPs, two main steps have to be followed [9]. First, a joint distribution over all quantities of interest $(\mathbf{y}, \mathbf{f}_*)^\mathrm{T}$, also called prior distribution, is defined as:

$$\begin{pmatrix} \mathbf{y} \\ \mathbf{f}_* \end{pmatrix} \sim \mathcal{N}\left(\begin{pmatrix} m(X) \\ m(X_*) \end{pmatrix}, \begin{pmatrix} K(X,\, X) + \sigma_\varepsilon^2\, I & K(X,\, X_*) \\ K(X_*,\, X) & K(X_*,\, X_*) \end{pmatrix}\right) \tag{A6}$$

whereby [9]:

$$m(X) \;= \mathbb{E}\,(\mathbf{y}) \tag{A7}$$

$$m(X_*)(\mathbf{f}_*) \tag{A8}$$

$$K(X,\, X) + \sigma_\varepsilon^2 I = Cov(\mathbf{y},\, \mathbf{y}) \tag{A9}$$

$$K(X_*\,,\, X) \;=\; Cov(\mathbf{f}_*,\, \mathbf{y}) \tag{A10}$$

$$K(X,\, X_*) \;=\; Cov(\mathbf{y},\, \mathbf{f}_*) \tag{A11}$$

$$K(X_*,\, X_*) \;=\; Cov(\mathbf{f}_*\,,\, \mathbf{f}_*) \tag{A12}$$

Second, after observing data, the observations can be combined with the prior distribution using Bayes' rule to determine the posterior distribution p of $\mathbf{f}_*$, which is, again, Gaussian [9]:

$$p(\mathbf{f}_* \,\big|\, X,\, \mathbf{y},\, X_*) \;=\; (\mathbf{f}_* \;\; (\mathbf{f}_*\,,\, \mathbf{y},\, X_*),\, Cov(\mathbf{f}_* \,\big|\, X,\, \mathbf{y},\, X_*)) \tag{A13}$$

$$\mathbb{E}\left(\mathbf{f}_* \,\middle|\, X,\, \mathbf{y},\, X_*\right) = m(X_*) + K(X_*,\, X)\left[K\left(X,\, X\right) + \sigma_\varepsilon^2 I\right]^{-1}\,\left(\mathbf{y} - m(X)\right) \tag{A14}$$

$$Cov(\mathbf{f}_* \,\middle|\, X,\, \mathbf{y},\, X_*) = K(X_*,\, X_*) - K(X_*,\, X)\left[K\left(X,\, X\right) + \sigma_\varepsilon^2\, I\right]^{-1}\, K(X,\, X_*) \tag{A15}$$

$\mathbb{E}\left(\mathbf{f}_* \mid X, \mathbf{y}, X_*\right)$ is the predicted value of the model from the given data set. This result shows the advantage of applying Gaussian process regression. Instead of a point estimate for the unknown values $\mathbf{f}_*$, the entire probability distribution can be evaluated. Furthermore, if $m(X)$ and $m(X_*)$ are set to zero, which is very common [9], the prediction depends largely on the selected covariance function (see Equation (A14)).

Hence, the covariance function is fundamental to the performance of the model. Depending on the existing structure in the data, different covariance functions are more suitable than others. Covariance functions are parameterized by a set of hyperparameters $\boldsymbol{\theta}$. Different covariance functions have different hyperparameters $\boldsymbol{\theta}$ [9]. In the following, the covariance functions used in this work are introduced.

First, the radial basis function (RBF) was used, which is probably the most widely applied covariance function [9]. It has the form [9]:

$$k(\mathbf{x},\, \mathbf{x}') = \sigma_f^2 \cdot \exp\left(-\frac{|\mathbf{x} - \mathbf{x}'|^2}{2l^2}\right) \tag{A16}$$

where σ_f and l are hyperparameters.

Second, the rational quadratic (RQ) covariance function which is defined by [9]:

$$k(\mathbf{x},\, \mathbf{x}') = \sigma_f^2 \cdot \left(1 + \frac{|\mathbf{x} - \mathbf{x}'|^2}{2\alpha l^2}\right)^{-\alpha},\ \alpha > 0, \tag{A17}$$

was applied. The hyperparameters are σ_f, α, and l.

Third, the Matérn 5/2 covariance function was employed, which is given by [9,33]:

$$k(\mathbf{x},\, \mathbf{x}') = \sigma_f^2 \left(1 + \frac{\sqrt{5}\,|\mathbf{x} - \mathbf{x}'|}{l} + \frac{5\,|\mathbf{x} - \mathbf{x}'|^2}{3 \cdot l^2}\right) \cdot \exp\left(-\frac{\sqrt{5}\,|\mathbf{x} - \mathbf{x}'|}{l}\right). \tag{A18}$$

The Matérn 5/2 covariance function has the two hyperparameters σ_f and l.

Higher-dimensional models can be designed in a flexible way if they are constructed by multiplying one-dimensional covariance functions for each input dimension. If, for each input dimension d, a single, one-dimensional RBF covariance function is defined, each dimension d has its own hyperparameters. This results in the RBF-ARD covariance function, which can be expressed formally with (compare Equation (A16)) [34]:

$$k(\mathbf{x},\, \mathbf{x}') = \prod_{d=1}^{D} \sigma_d^2 \cdot \exp\left(-\frac{\left(\mathbf{x}_d - \mathbf{x}'_d\right)^2}{2l_d^2}\right) = \sigma_\mathbf{f}^2 \cdot \exp\left(-\frac{1}{2}\sum_{d=1}^{D}\frac{\left(\mathbf{x}_d - \mathbf{x}'_d\right)^2}{l_d^2}\right) \tag{A19}$$

With this special covariance function, automatic relevance determination (ARD) can be conducted, because the values of the hyperparameters length-scale $l_1, l_2, \ldots, l_D$ determine the relevance of the corresponding input variable. Input dimensions d with large length-scale l_d imply little variation along the different dimensions d and hence are less important for the predicted outcome $\mathbf{f}_*$. [35]

Fourthly, an approach presented by Duvenaud et al. [18] was employed, called additive GP, that allows the consideration of interaction between different input dimensions d. The n-th order additive covariance function is defined as [18]:

$$k(\mathbf{x},\, \mathbf{x}') = \sigma_n^2 \sum_{1 \le i_1 < i_2 < \ldots < i_n \le D}\left[\prod_{d=1}^{n} k_{i_d}(\mathbf{x}_{i_d},\, \mathbf{x}'_{i_d})\right], \tag{A20}$$

where D is the dimension of the input space, and σ_n^2 is the variance of the n-th order. In particular, the D-th order additive covariance function is a product of each dimension's covariance function [18]:

$$k(\mathbf{x},\ \mathbf{x}') = \sigma_D^2 \prod_{d=1}^{D} k_d\left(\mathbf{x}_d,\ \mathbf{x}'_d\right) \tag{A21}$$

In the case where each base covariance function is an RBF covariance function, the D-th order term corresponds to the multivariate RBF-ARD covariance function (see Equation (A19)). The only design choice for additive covariance functions is the selection of the one-dimensional base covariance functions for each input dimension d.

Finally, a closed form covariance function for automatic pattern discovery and extrapolation, introduced by Wilson et al. [19] and called spectral mixture (SM) covariance function, was utilized in the present work. This covariance function is derived by modelling the spectral density of covariance functions (its Fourier transform) using scale-location mixtures of Gaussians.

References

1. Colligan, K.J. The friction stir welding process: An Overview. In *Friction Stir Welding—From Basics to Applications*; Lohwasser, D., Chen, Z., Eds.; Woodhead Publishing Limited and CRC Press LLC: Cambridge, UK, 2010; pp. 15–41. ISBN 978-1-84569-450-0.
2. Thomas, W.M.; Nicholas, E.D.; Needham, J.C.; Murch, M.G.; Temple-Smith, P.; Dawes, C.J. Improvements Relating to Friction Welding. European Patent Specifications 0 615 480 B1, 8 November 1995.
3. Taheri, H.; Kilpatrick, M.; Norvalls, M.; Harper, W.J.; Koester, L.W.; Bigelow, T.; Bond, L.J. Investigation of Nondestructive Testing Methods for Friction Stir Welding. *Metals* **2019**, *9*, 624. [CrossRef]
4. Sagar, S.P.; Miyasaka, C.; Ghosh, M.; Tittmann, B.R. NDE of friction stir welds of Al alloys using high-frequency acoustic microscopy. *Nondestruct. Test. Eval.* **2012**, *27*, 375–389. [CrossRef]
5. Mishra, D.; Roy, R.B.; Dutta, S.; Pal, S.K.; Chakravarty, D. A review on sensor based monitoring and control of friction stir welding process and a roadmap to Industry 4.0. *J. Manuf. Process.* **2018**, *36*, 373–397. [CrossRef]
6. Yunus, M.; Alsoufi, M.S. Mathematical Modelling of a Friction Stir Welding Process to Predict the Joint Strength of Two Dissimilar Aluminium Alloys Using Experimental Data and Genetic Programming. *Model. Simul. Eng.* **2018**, 1–18. [CrossRef]
7. Pathak, M.; Jaiswal, D. Applications of Artificial Neural Networks in Friction Stir Welding: A Review. *Int. J. Technol. Explor. Learn.* **2014**, *3*, 513–517.
8. Verma, S.; Gupta, M.; Misra, J.P. Performance evaluation of friction stir welding using machine learning approaches. *MethodsX* **2018**, *5*, 1048–1058. [CrossRef] [PubMed]
9. Rasmussen, C.E.; Williams, C.K.I. *Gaussian Processes for Machine Learning*; MIT Press: Cambridge, MA, USA, 2006; ISBN 026218253X.
10. Schoelkopf, B.; Smola, A.J. *Learning with Kernels: Support Vector Machines, Regularization, Optimization, and Beyond*; MIT Press: Cambridge, MA, USA, 2002; ISBN 9780262194754.
11. Fahrmeir, L.; Kneib, T.; Lang, S.; Marx, B. *Regression. Models, Methods and Applications*; Springer: Dordrecht, The Netherlands, 2013; ISBN 978-3-642-34333-9.
12. Üstün, B.; Melssen, W.J.; Buydens, L.M.C. Facilitating the application of Support Vector Regression by using a universal Pearson VII function based kernel. *Chemom. Intell. Lab. Syst.* **2006**, *81*, 29–40. [CrossRef]
13. Zuo, L.; Zuo, D.; Zhu, Y.; Wang, H. Effect of process parameters on surface topography of friction stir welding. *Int. J. Adv. Manuf. Technol.* **2018**, *98*, 1807–1816. [CrossRef]
14. Huang, W.; Kovacevic, R. A laser-based vision system for weld quality inspection. *Sensors* **2011**, *11*, 506–521. [CrossRef] [PubMed]
15. Hartl, R.; Bachmann, A.; Liebl, S.; Zens, A.; Zaeh, M.F. Automated surface inspection of friction stir welds by means of structured light projection. In Proceedings of the 21st Chemnitz Seminar on Materials Engineering, Chemnitz, Germany, 6–7 March 2019; 2019; p. 12035. [CrossRef]

16. Hartl, R.; Praehofer, B.; Zaeh, M.F. Prediction of the surface quality of friction stir welds by the analysis of process data using Artificial Neural Networks. *Proc. Inst. Mech. Eng. Part L J. Mater. Des. Appl.* **2020**, *234*, 732–751. [CrossRef]
17. Hartl, R.; Vieltorf, F.; Zaeh, M.F. Correlations between the Surface Topography and Mechanical Properties of Friction Stir Welds. *Metals* **2020**, *10*, 890. [CrossRef]
18. Duvenaud, D.; Nickisch, H.; Rasmussen, C.E. Additive Gaussian Processes. In *Advances in Neural Information Processing Systems 24, Neural Information Processing Systems 2011 (NIPS 2011), Granada Congress and Exhibition Centre, Granada, Spain, 12–17 December 2011*; Shawe-Taylor, J., Zemel, R.S., Bartlett, P.L., Pereira, F., Weinberger, K.W., Eds.; Neural Information Processing Systems Foundation: La Jolla, CA, USA, 2011.
19. Wilson, A.G.; Adams, R.P. Gaussian Process Kernels for Pattern Discovery and Extrapolation. In *International Conference on Machine Learning (ICML), JMLR W&CP 28(3), Proceedings of the International Conference on Machine Learning, Atlanta, GA, USA, 17–19 June, 2013*; Dasgupta, S., McAllester, D., Eds.; International Machine Learning Society: Princeton, NJ, USA, 2013; pp. 1067–1075.
20. Hesse, W. *Key to Aluminum Alloys*, 12th ed.; fully revised; Beuth Verlag GmbH: Berlin, Germany; Wien, Austria; Zürich, Switzerland, 2016; ISBN 978-3-410-26873-4.
21. Krutzlinger, M.; Bachmann, A.; Wirth, F.X.; Roth, A.; Sünger, S.; Pieczona, S.J.; Zaeh, M.F. Implementierung Einer Messsensorik in ein Fräsbearbeitungszentrum zur Ermittlung Der Prozesskräfte und des Prozessmoments Beim Rührreibschweißen (Translated Title: "Implementation of a measuring system in a milling machining center to determine the process forces and the process torque during friction stir welding"). In *DVS Congress 2015, Proceedings of the Große Schweißtechnische Tagung, Nuremberg, Germany, 15–17 September 2015*; DVS—German Welding Society, Ed.; DVS Media: Duesseldorf, Germany, 2015; pp. 209–214. ISBN 9783945023464.
22. Costanzi, G.; Bachmann, A.; Zaeh, M.F. Entwicklung eines FSW-Spezialwerkzeugs zur Messung der Schweißtemperatur (Translated title: "Development of a FSW special tool for measuring the welding temperature"). In *DVS Congress 2017, Proceedings of the DVS Congress, Duesseldorf, Germany, 26–29 September 2017*; DVS—German Welding Society, Ed.; DVS Media GmbH: Duesseldorf, Germany, 2017; pp. 119–125. ISBN 9783961440085.
23. Bachmann, A.; Krutzlinger, M.; Zaeh, M.F. Influence of the welding temperature and the welding speed on the mechanical properties of friction stir welds in EN AW-2219-T87. In Proceedings of the 20th Chemnitz Seminar on Materials Engineering, Chemnitz, Germany, 14–15 March 2018. [CrossRef]
24. Richter, B. Robot-based Friction Stir Welding for E-mobility and General Applications. *Biul. Inst. Spaw. W Gliwicach* **2017**, *5*, 103–110. [CrossRef]
25. German Institute for Standardization. *Geometrical Product Specifications (GPS)—Surface Texture: Areal—Part 2: Terms, Definitions and Surface Texture Parameters*; Beuth Verlag GmbH: Berlin, Germany, 2012; DIN EN ISO 25178-2.
26. Brenner, P.; Kostron, H. Über die Vergütung der Aluminium-Magnesium-Silizium-Legierungen (Translated title: "On the tempering of aluminium-magnesium-silicon alloys"). *Z. Metallkde.* **1939**, *31*, 89–97.
27. German Institute for Standardization. *Testing of Metallic Materials—Tensile Test Pieces*; Beuth Verlag GmbH: Berlin, Germany, 2016; DIN 50125.
28. German Institute for Standardization. *Destructive Tests on Welds in Metallic Materials—Transverse Tensile Test*; Beuth Verlag GmbH: Berlin, Germany, 2013; DIN EN ISO 4136.
29. German Institute for Standardization. *Metallic Materials—Tensile Testing—Part. 1: Method of Test at Room Temperature*; Beuth Verlag GmbH: Berlin, Germany, 2017; DIN EN ISO 6892-1.
30. Vander Voort, G.F. *Metallography and Microstructures*, 9th ed.; ASM International: Almere, The Netherlands, 2004; ISBN 978-0871707062.
31. Haerdle, W.; Klinke, S.; Roenz, B. *Introduction to Statistics. Using Interactive MM*Stat. Elements*; Springer: Cham, Switzerland, 2015; ISBN 9783319177045.
32. Bachmann, A.; Gigl, T.; Hugenschmidt, C.P.; Zaeh, M.F. Characterization of the microstructure in friction stir welds of EN AW-2219 using coincident Doppler-broadening spectroscopy. *Mater. Charact.* **2019**, *149*, 143–152. [CrossRef]
33. Whitley, E.; Ball, J. Statistics review 2: Samples and populations. *Crit. Care* **2002**, *6*, 143–148. [CrossRef] [PubMed]

34. SheffieldML. Available online: https://github.com/SheffieldML/GPy/blob/40137cc8f7e0794bff55639ec55d4884c72e86b5/GPy/kern/src/coregionalize.py (accessed on 24 March 2020).
35. Duvenaud, D. Automatic Model Construction with Gaussian Processes. Doctoral Thesis, University of Cambridge, Cambridge, UK, 2014. [CrossRef]